Fermilab FERMILAB-Conf-01/380 January 2002

Development and Test of Single-Bore Cosϑ Nb_3Sn Dipole Models With Cold Iron Yoke

N. Andreev, G. Ambrosio, E. Barzi, R. Carcagno, D.R. Chichili, J. DiMarco, S. Feher, L. Imbasciati, V.V. Kashikhin, M. Lamm, P.J. Limon, D. Orris, P. Schlabach, C. Sylvester, M. Tartaglia, I. Terechkine, J.C. Tompkins, S. Yadav, R. Yamada, A.V. Zlobin

[1]***Abstract*--Two short Nb_3Sn dipole models based on a single-bore cos-theta coil with a cold iron yoke were fabricated and tested at Fermilab. This paper summarizes the details of magnet design and fabrication procedure, and reports the test results including quench performance and quench heater studies, and the magnetic measurements.**

***Index Terms*—superconducting magnet, design, technology**

I. Introduction

HIGH field accelerator magnets are being developed at Fermilab for the next generation of hadron colliders. These magnets are designed for a nominal field of 10-12 T in the magnet bore of 40-50 mm at the operating temperature of 4.3 K and are based on various design and fabrication approaches [1],[2]. One of the approaches being explored for these magnets is based on Nb_3Sn cos-theta coils and wind-and-react techniques.

The magnetic and mechanical design of a single-bore short model with cold iron yoke based on this approach was developed and described in [3]. A model magnet program to validate and optimize the magnet design and fabrication technologies has been undertaken. Two 1 m long model magnets (HDFA02 and HFDA03) were recently fabricated and tested in the Fermilab Vertical Magnet Test Facility. The results of these tests as well as magnet design features and details of fabrication procedures are reported in this paper.

II. Magnet Design

The baseline design consists of a two-layer shell-type coil with a 43 mm bore and a cold iron yoke. Fig. 1 shows both a 3D view of the magnet and the assembled magnet cold mass.

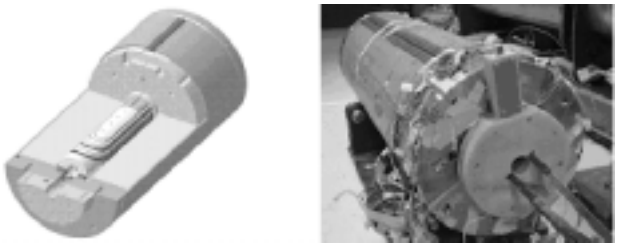

Fig. 1. Short model 3D view and assembled cold mass.

[1] Manuscript received September 24, 2001.
This work was supported by the U.S. Department of Energy.
Authors are with Fermilab, MS-316, P.O. Box 500, Batavia, IL 60510, USA (e-mail: zlobin@fnal.gov).

Both models utilize the same keystone Rutherford-type cable made of 28 Nb_3Sn strands, each 1 mm in diameter. The cable has a 25 μm thick stainless steel core to control crossover resistance. A 0.125 mm thick ceramic tape impregnated with liquid ceramic binder was used for cable insulation. The Nb_3Sn strands were produced by Oxford Superconducting Technology (OST) using the Modified Jelly Roll (MJR) process. The critical current for virgin strands measured at 12 T and 4.2 K was 726 A, and for extracted strands, 665 A. The critical current degradation in the cable is 8.5%. The measured strand RRR was within a 7-19 range.

Each half-coil consists of 24 turns, 11 turns in the inner layer and 13 turns in the outer layer. The inner layer and the outer layer pole inserts, and four spacers per quadrant, two for each layer, minimize the low order geometrical harmonics in the magnet body. The coil ends also have a blockwise turn layout with the same number of blocks and turns in the block as in the magnet body.

Two layers of each half-coil were wound and cured using a single piece of cable without an interlayer splice. Quench protection heaters were installed before heat treatment on the coil outer surface in between the layers of ground insulation. The half-coils were reacted using a three-step temperature cycle and then were impregnated with epoxy.

The coil fabrication technology utilizes the wind-and-react approach. In order to simplify coil fabrication and reduce magnet cost some new features have been introduced in the fabrication process. The cable and each half-coil is impregnated with a liquid ceramic binder and cured at 120C. After winding, pre-forming, curing, and coil size measurements the two half-coils were assembled, reacted and epoxy impregnated together. This approach allows easy coil handling, coil size and field quality control before the final magnet assembly, and avoids expensive collars and a delicate collaring procedure. The other details of the short model fabrication are reported elsewhere [4].

Wind-and-react techniques impose demanding requirements on the magnet insulation which must withstand a long heat treatment at high temperature under compression. The ceramic insulation meets these requirements and was used in both models with an inorganic ceramic binder (CTD Inc.) in order to improve cable insulation stiffness before coil winding and to pre-form the coils during coil curing. The details of magnet insulation design and its properties are reported elsewhere [5].

Complicated end parts, used in cos-theta coils, in case of Nb_3Sn magnets and wind-and-react techniques have to

withstand the coil heat treatment without deformation and match the cable shape in the ends to avoid shorts. An optimization method for metal end parts was developed and successfully used together with rapid prototyping techniques [6]. This approach reduced the time and the cost of end part optimization processes. Water jet machining was used for end part fabrication resulting in the reduction of their costs by a factor of 2.5 and manufacturing time by a factor of 10 while providing acceptable part quality.

The support structure of the models consists of a vertically split iron yoke locked by two aluminum clamps and an 8-mm thick stainless steel skin. Aluminum spacers between the coils and the iron yoke prevented excessive compression of the coils during magnet assembly. The coil prestress is provided by the clamps and the skin. The iron yoke has an inner diameter of 120 mm and an outer diameter of 400 mm. Two 50 mm end plates provide axial coil prestress and restrict the longitudinal motion of coil ends under the Lorentz forces.

III. Quench Performance

The models were tested in boiling liquid helium at 4.5 K. HFDA02 had voltage taps installed on the each half-coils and across all Nb_3Sn/NbTi lead splices. In HFDA03 two additional voltage taps were added in order to detect quenches in the inner and outer layer of each half-coil.

Coil azimuthal stresses and longitudinal end forces in both models were measured during fabrication and during cold test in each excitation cycle using resistive and capacitive gauges. Azimuthal coil prestress and longitudinal end prestress remained at 4.5 K after cooling down. Moreover, the strain gauge data indicated no unloading of the coil up to the maximum reached currents. Coil deformation due to the Lorentz force was elastic throughout the test current range.

A. Magnet training

The training results at 4.5 K in first thermal cycle for HFDA02 and HFDA03 are presented in Fig. 2. The quench performance of both magnets was very similar. The maximum achieved current was less than 10 kA which is a factor of two smaller than the expected magnet critical current. During training, the magnets were excited with different current ramp rates. No noticeable effect on the magnet quench performance was found.

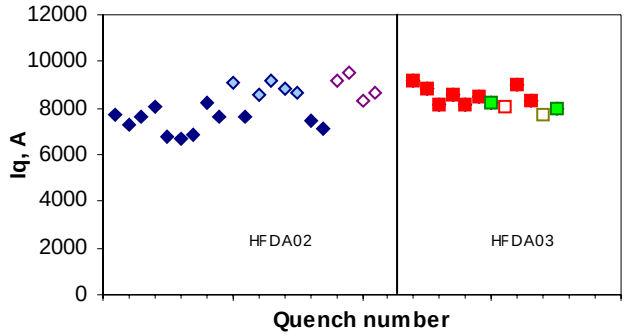

Fig. 2. HFDA02 and HFDA03 training at 4.5 K. Quenches with different current ramp rates (20, 100, 200, 300 and 500 A/s) are shown.

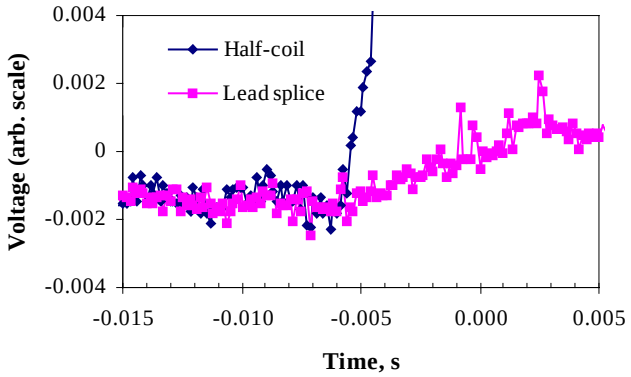

Fig. 3. Typical voltage taps data during magnet quench.

All quenches in both magnets occurred in the Nb_3Sn coil leads just near their splices with the NbTi cables. It is confirmed by the signals from the voltage taps installed on the coils and in the splice regions (see data in Fig. 3). The quenches never occurred in the magnet coils. The possible causes of the observed quench performance including Ic degradation of the Nb_3Sn cable in the splice region during coil reaction, cable mechanical damage during splicing and magnet assembly are being studied.

B. Heater induced quenches

Both magnets have two sets of quench heaters installed on the outer coil surface. Each heater consists of four 0.025 mm thick and 12 mm wide stainless steel strips connected in series and placed one in each quadrant. The time delay between heater firing and coil quench vs. heater voltage at I=4100 A and vs. magnet current at U_{qh}=400 V is shown in Fig.4 and 5.

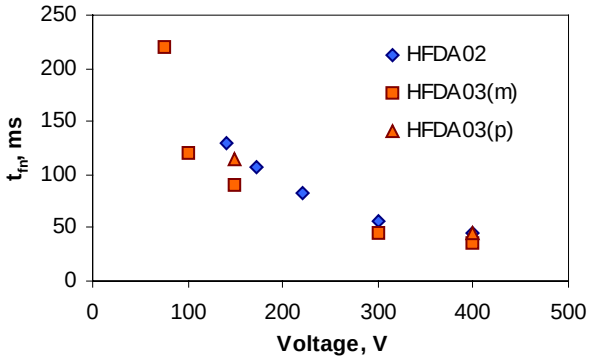

Fig. 4. Heater time delay t_{fn} vs. the voltage applied to heater at I=4100 A.

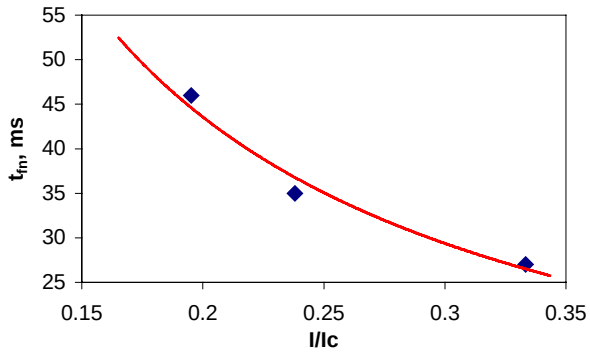

Fig. 5. Heater time delay t_{fn} vs. the normalized magnet current at U_{qh}=400 V.

As it can be seen, even at low currents the measured heater time delay is small. Extrapolation to the currents corresponding to the fields of 10-11 T and 10% critical current margin shows that heater efficiency in Nb_3Sn magnets is rather high (t_{fn}~20 ms) as in the NbTi accelerator magnets.

IV. Magnetic Measurements

Warm magnet transfer functions (B/I) of 0.6154 (HFDA02) and 0.6168 T/kA (HFDA03) and cold ones of 0.6154 (HFDA02) and 0.6180 T/kA (HFDA03) measured at 10 A and 6 kA in the straight section agree well with that expected from the design of 0.6140 and 0.6155 T/kA respectively. The measured magnetic length of 0.803±0.005 m is also in good agreement with the calculated value of 0.809 m.

The field in magnet body is represented in terms of harmonic coefficients defined by the power series expansion

$$B_y + iB_x = B_1 \times 10^{-4} \sum_{n=1}^{\infty} (b_n + ia_n) \left(\frac{x + iy}{r_0} \right)^{n-1},$$

where B_x and B_y are the transverse field components, B_1 is the dipole field, b_n and a_n are the normalized harmonic coefficients ($b_1=10^4$) at a reference radius r_0 of 10 mm.

A. Geometrical harmonics

The geometrical harmonics measured at 3 kA in the magnet body and calculated for the design geometry are presented in Table I. A noticeable improvement of field quality in HFDA03 with respect to HFDA02 can be seen. It was achieved by better shimming of the HFDA03 coil during impregnation and yoking. However, some of the low order harmonics exceed 3 sigma of RMS field errors expected due to possible 50 μm coil block displacements. These are due to asymmetry and shift of coil midplanes during reaction which at present time may be as large as 0.2-0.5 mm. Optimizing the reaction and impregnation tooling will reduce this effect.

Table I:
Geometrical harmonics in magnet body (I=3000A)

n	Design values		HFDA02		HFDA03	
	$\sigma_{an,bn}$	b_n	a_n	b_n	a_n	b_n
2	1.20	-	-9.6	4.1	1.93	-7.13
3	0.56	0.00	-0.2	-4.0	0.81	-2.36
4	0.28	-	-1.1	0.4	-0.75	-0.19
5	0.10	0.00	0.3	0.0	0.04	-0.53
6	0.05	-	0.3	0.0	0.03	0.12
7	0.02	0.00	-0.1	0.1	0.03	0.04
8*	0.01	-	-	-	-	-
9	0.00	-0.09	-0.2	-0.2	0.04	-0.01

*The measured a_8/b_8 data were used for the centering correction.

B. Coil magnetization

The effect of coil magnetization on the normal sextupole measured and calculated [7] in these magnets is shown in Fig. 6. Calculations of the magnetization harmonics reproduce the measured values over a wide range of currents. The width of the sextupole hysteresis loop is large (~50 units) at 1 kA due to the high critical current density and large effective filament diameter that reaches ~100 μm in Nb_3Sn strands produced using MJR process [8].

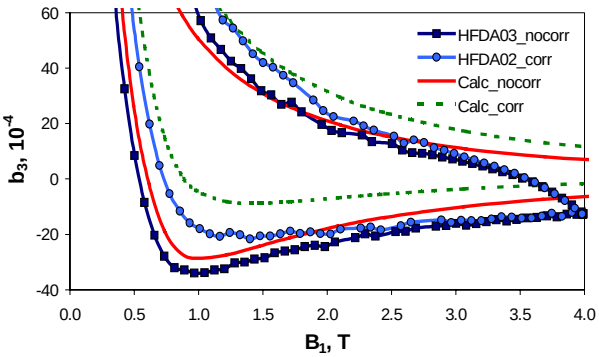

Fig. 6. Measured and calculated normal sextupole.

To reduce the coil magnetization effect in Nb_3Sn accelerator magnets, simple passive correctors based on thin iron strips were proposed [7]. To verify this approach HFDA02 was tested in the second thermal cycle with a simple model of such a corrector. Four iron strips 0.1 mm thick and 15.85 mm wide were placed between two layers of epoxy impregnated fiberglass tape, wrapped on the mandrell and then cured. The produced G10 tube was installed in the magnet bore such that the iron strips were at a radius of 21.4 mm and in the right position azimuthally (55.2 degree from the coil midplane). Measured and calculated sextupole loops in HFDA02 are presented in Fig.6. Data characterizing the corrector efficiency, shown in Table II, validate this correction technique.

Table II:
Passive corrector efficiency.

	Before correction		After correction		Correction factor	
	calc	meas	calc	meas	calc	meas
$b_3(4T) - b_3(1.5T)$	16.9	15.8	6.6	7.9	2.6	2.0
$b_5(4T) - b_5(1.5T)$	2.36	2.36	1.36	1.36	1.7	1.7

C. Harmonics decay and "snapback"

To check for dynamic effects during injection, measurements were performed during a current plateau at 3 kA and at 1.75 kA. The plateau was preceded by two cycles in which the magnet was ramped 0-6500-0 A at a ramp rate of 40 A/s. The time dependence of the normal sextupole at the injection plateau for HFDA02 and HFDA03 is presented in Fig. 7. Changes in the harmonics during injection are very small (<1 unit) with respect to those observed in NbTi accelerator magnets [9].

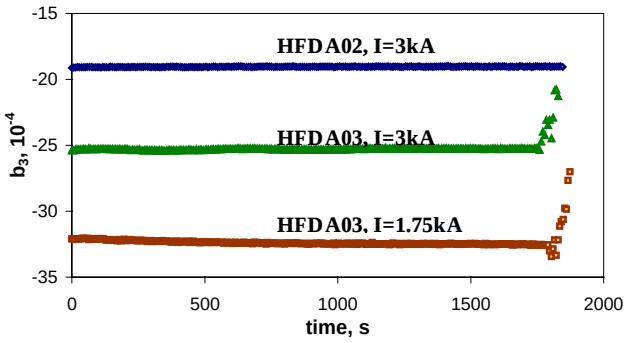

Fig. 7. Time dependence of b_3 at the injection. The current ramp stops at t=0. The first few measurements after ramping is resumed are also plotted.

D. *Eddy current effects*

Nb_3Sn magnets fabricated using the wind-and-react technique typically show large eddy current effects due to the small crossover resistance created in the cable during coil reaction [10]. To increase the crossover resistance, the cable in these magnets has a 25 μm stainless steel core. However, Fig. 8 shows a noticeable eddy current effect in the measured magnet transfer function B/I. Analysis has shown that it is related to the large eddy currents induced in the Al spacers placed between the coil and the iron yoke. Meanwhile, the eddy current effect in the sextupole (see Fig.9) and other low-order allowed harmonics is small due to high crossover resistance in the cable. It is also consistent with the results of AC loss measurements shown in Fig.10.

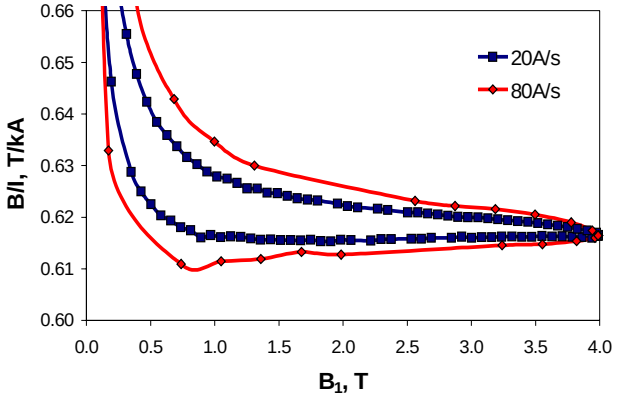

Fig. 8. Magnet transfer function B/I measured at different ramp rates.

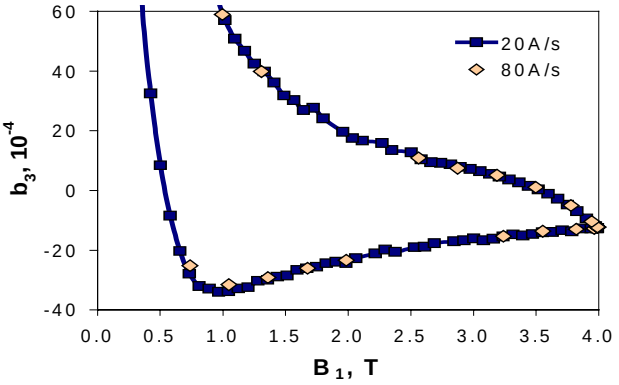

Fig. 9. Sextupole harmonics b_3 measured at different ramp rates.

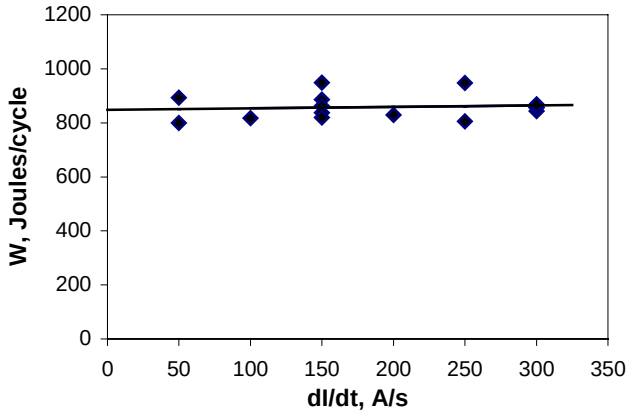

Fig. 10. AC loss measured in the triangular cycles 500-6500-500 A with different current ramp rates (HFDA03).

V. Conclusions

Two Nb_3Sn dipole short models were fabricated and tested recently at Fermilab. The low maximum quench current reached in both models was restricted by the quenches in the lead splices area. The possible causes of that are being investigated including mechanical damages or degradation of Nb_3Sn coil leads during magnet fabrication. Quench heaters tested in both models demonstrated a high efficiency comparable with the heater efficiency in NbTi accelerator magnets.

Field quality measurements of Nb_3Sn dipole models are consistent with expectations. Large low-order geometrical harmonics are explained by the deviation of coil geometry from the design. Improvements will be achieved by modifying the coil fabrication tooling and procedures. The relatively large measured magnetization harmonics are consistent with calculations based on the properties of Nb_3Sn strand used in these models. A scheme to minimize this effect with passive correction shims was successfully tested. The noticeable sextupole decay and "snapback" effect observed in NbTi accelerator magnets at injection has not been found in those tested Nb_3Sn dipole models. This is not yet understood and will be studied further in future models. A stainless steel core in the cable has apparently eliminated large eddy current effects seen in other Nb_3Sn magnets. Further fabrication and tests of models in this design series will be continued.

VI. Acknowledgment

Authors would like to thank engineers and technicians of Fermilab's Technical Division for contributions to this work, and R.M. Scanlan and H. Higley (LBNL) for fabrication of cable for these models.

VII. References

[1] A.V. Zlobin et al., "Development of Cos-theta Nb_3Sn Dipole Magnets for VLHC", paper RPPH085, PAC2001, Chicago, IL June 2001.

[2] G. Ambrosio et al., "Design and Development of Single-Layer Common Coil Nb_3Sn Dipole Magnet for VLHC", paper RPPH079, PAC2001, Chicago, IL June 2001.

[3] G. Ambrosio et al., "Development of the 11 T Nb_3Sn Dipole Model at Fermilab", IEEE Transaction on Applied Superconductivity, Vol. 10, No. 1, March 2000, p.298.

[4] D.R. Chichili et al., "Fabrication of the Shell-Type Nb_3Sn Dipole Model at Fermilab", IEEE Transaction on Applied Supercon-ductivity, Vol. 11, No. 1, March 2001, p. 2160.

[5] N.I. Andreev et al., "Development and Study of Insulation Systems for Nb_3Sn Accelerator Magnets", *this conference*.

[6] S. Yadav et al., "Coil Design Issues for the High Field Dipole at Fermilab", IEEE Transactions on Applied Superconductivity, Vol. 11, No. 1, March 2001, p. 2284.

[7] V.V. Kashikhin and A.V. Zlobin, "Correction of the Persistent Current Effect in Nb_3Sn Dipole Magnets", IEEE Transactions on Applied Superconductivity, Vol. 11, No. 1, March 2001, p. 2058.

[8] E. Barzi et al., "Study of Nb_3Sn Strands for Fermilab's High Field Dipole Models", IEEE Transaction on Applied Superconductivity, Vol. 11, No. 1, March 2001, p. 3595.

[9] L. Bottura et al., "Performance of the LHC Final Design Full Scale Superconducting Dipole Prototypes", IEEE Transaction on Applied Superconductivity, Vol. 11, No. 1, March 2001, p. 1554.

[10] A. den Ouden et al., "Application of Nb_3Sn Superconductors in High-field Accelerator Magnets", IEEE Transaction on Applied Superconductivity, Vol. 7, No. 2, June 1997, p. 733.